Available online at www.sciencedirect.com
ScienceDirect
Journal of Power Sources 178 (2008) 188–196
JOURNAL OF POWER SOURCES
www.elsevier.com/locate/jpowsour

Modeling of PEM fuel cell Pt/C catalyst degradation

Wu Bi [a,*], Thomas F. Fuller [a,b]

[a] School of Chemical and Biomolecular Engineering, Georgia Institute of Technology, Atlanta, GA 30332, USA
[b] Center for Innovative Fuel Cell and Battery Technologies, Georgia Tech Research Institute, Georgia Institute of Technology, Atlanta, GA 30332, USA

Received 15 October 2007; received in revised form 4 December 2007; accepted 5 December 2007
Available online 14 December 2007

Abstract

Pt/C catalyst degradation remains as one of the primary limitations for practical applications of proton exchange membrane (PEM) fuel cells. Pt catalyst degradation mechanisms with the typically observed Pt nanoparticle growth behaviors have not been completely understood and predicted. In this work, a physics-based Pt/C catalyst degradation model is proposed with a simplified bi-modal particle size distribution. The following catalyst degradation processes were considered: (1) dissolution of Pt and subsequent electrochemical deposition on Pt nanoparticles in cathode; (2) diffusion of Pt ions in the membrane electrode assembly (MEA); and (3) Pt ion chemical reduction in membrane by hydrogen permeating through the membrane from the negative electrode. Catalyst coarsening with Pt nanoparticle growth was clearly demonstrated by Pt mass exchange between small and large particles through Pt dissolution and Pt ion deposition. However, the model is not adequate to predict well the catalyst degradation rates including Pt nanoparticle growth, catalyst surface area loss and cathode Pt mass loss. Additional catalyst degradation processes such as new Pt cluster formation on carbon support and neighboring Pt clusters coarsening was proposed for further simulative investigation.

Keywords: PEM fuel cells; Platinum catalyst degradation; Physical model; Platinum oxidation; Platinum dissolution; Pt ion diffusion

1. Introduction

Over the last decade remarkable developments have been made in fundamental understanding, materials development, and systems engineering of proton exchange membrane (PEM) fuel cells. Nonetheless, cost and durability are barriers that must be overcome before PEM fuel cells are introduced commercially. Perhaps the most aggressively pursued application is the transportation market. Here, the fuel cell stack is subjected to a large number of potential cycles, and durability of fuel cell components, including the platinum catalyst, remains as one of the primary limitations for PEM fuel cells. Good understanding of fuel cell degradation processes can lead to the development of new fuel cell materials providing improved performances and prolonged lifetimes.

Carbon-supported platinum or its alloys have the best kinetics for oxygen reduction and the best electrode performance for low temperature acid fuel cells. At the same time, platinum has a small but finite solubility [1–3] under the highly acidic and oxidizing cathodic environment of PEM fuel cells. Carbon-supported platinum catalyst degrades through dissolution [4–6], which is a process accelerated by potential cycling. Platinum surface atoms on nanoparticles can be oxidized by both water and oxygen at cathode [7–11]. At high humidity fuel cell conditions, platinum oxidation by water is dominant [11]. With techniques of electrochemical quartz-crystal nanobalance, cyclic-voltammetry and Auger electron spectroscopy, Jerkiewicz's work [12] confirmed that anhydrous PtO instead of $Pt(OH)_x$ is the only oxidized form of Pt in the potential range of 0.85–1.4 V (vs. NHE) and that a surface PtO lattice formed by an interfacial place-exchange process at potentials of 1.1–1.2 V (vs. NHE).

From the PEM fuel cell cathode, dissolved Pt ions can be transported to other regions of the fuel cell. These dissolved Pt ions can be reduced electrochemically and deposited on existing Pt particles [13] within the cathode. These Pt ions can also diffuse away from the cathode into the membrane. Subsequently, hydrogen that permeates through the membrane from the anode can reduce the cations, forming a Pt "band" in the membrane. The Pt "band" position is determined by the rates of permeation

* Corresponding author. Tel.: +1 404 894 2834; fax: +1 404 894 2866.
E-mail address: wu.bi@chbe.gatech.edu (W. Bi).

0378-7753/$ – see front matter © 2007 Elsevier B.V. All rights reserved.
doi:10.1016/j.jpowsour.2007.12.007

of hydrogen and oxygen [2,14–16]. It is also possible that some dissolved platinum leaves the cell with the product water. However, the concentration of soluble Pt species in fuel cell product water has been determined at pg g^{-1} (ppt) levels in our tests by Inductively Coupled Plasma Mass Spectroscopy (ICPMS). These low amounts indicate that relative to the other mechanisms for platinum loss from the cathode a negligible amount of platinum leaves the fuel cell system.

Pt dissolution and re-deposition causes Pt catalyst structure morphological changes with a concomitant decrease in electrochemically active surface area and reduced activity for oxygen reduction. Processes of Pt dissolution from small particles, and Pt ion deposition on large particles result in increased mean particle size and widened Gaussian size distribution. However, the detailed mechanisms of Pt catalyst degradation have not been completely understood. Ferreira et al. [2] observed with TEM that the size distributions of carbon-supported Pt particles changed from a Gaussian distribution at the cathode surface region to a uniform distribution at the cathode/membrane interface. Also, the average particle size increased in the direction towards the interface. Other X-ray diffraction work by More and Reeves [17] showed that the Pt particle size distribution becomes "bi-modal," but with a large portion of the smallest particles still present after degradation tests. The authors believed that new small Pt particles were produced during the degradation processes. Also, coarsening of neighboring Pt clusters and/or nanoparticles is speculated even though PEM fuel cells operate at relatively low temperatures. Electrochemical reactions of Pt oxidation [7,8,18] and Pt dissolution [18] have been simulated with various forms of the Butler–Volmer equation.

The thrust of our research is to develop detailed physics-based models for degradation phenomena. From these models two objectives are pursued. First through a better understanding of the mechanisms and physical processes, provide a guide for the development of new materials and propose system-level approaches to mitigate degradation. The second objective is to predict life performance of catalyst systems under conditions appropriate for transportation applications, *i.e.*, hundreds of thousands of potential cycles over several thousands of hours of operation. More specifically, from a given cell potential and temperature as a function of time we seek to predict these observed phenomena: (1) the rate of platinum dissolution and diffusion in the membrane, (2) changes in electrochemical area (ECA), (3) the growth of particle size, and (4) the coverage of oxides. In addition, we hope to account for differences in durability that arise from changes in catalyst structure or alloying with well-defined and measurable kinetic and thermodynamic data. Furthermore, the general characteristics of these macroscopic models are (1) physics based, (2) well-defined and measurable quantities, (3) consistent with thermodynamics, and (4) limited number empirical or fitted parameters.

Darling and Meyers [19] proposed the first Pt/C catalyst degradation model for PEM fuel cells. This model used a two-particle size profile to simulate cathode surface area loss through Pt dissolution/deposition and Pt ion transport in membrane electrode assembly (MEA). Their model [19] predicted a decrease in size for both small and large particles after degradation. Also the model allowed the dissolved Pt ions from the cathode to be transported through membrane and further electrochemically deposited at the anode, which is more appropriate in phosphoric acid fuel cells, but is not typically observed in PEM fuel cell systems [14–16].

In this work, a Pt catalyst degradation model is proposed that builds on the earlier work of Darling and Meyers [19]. This new model includes some different features such as cathode Pt mass loss into membrane forming a Pt "band", as discussed earlier. Under the defined cathode potential temporal profiles, cathode platinum mass, catalyst particle size, and platinum surface area are predicted and compared to the experimental data, assisting further understanding catalyst degradation mechanisms.

2. Degradation model details

In this new simulation, catalyst degradation caused by Pt dissolution and deposition is modeled with three reactions: Pt electrochemical dissolution (Reaction 1) and Pt oxidation (Reaction 2), and diffusion of Pt ions and subsequent precipitation by hydrogen reduction (Reaction 3). This last reaction, precipitation of Pt ions in the membrane, is assumed to be irreversible and contributes to Pt mass loss from cathode. Chemical dissolution of Pt oxide (Reaction 4) is not considered due to the unclear kinetics. What is more, inclusion of this reaction does not affect the results measurably due to its most likely slow kinetics [18].

$$Pt = Pt^{2+} + 2e^- \quad (U_1^0 = 1.188\,V\ [1]) \qquad \text{(Reaction 1)}$$

$$Pt + H_2O = PtO + 2H^+ + 2e^- \quad (U_2^0 = 0.98\,V\ [2]) \qquad \text{(Reaction 2)}$$

$$Pt^{2+} + H_2 = Pt + 2H^+ \qquad \text{(Reaction 3)}$$

$$PtO + 2H^+ = Pt^{2+} + H_2O \qquad \text{(Reaction 4)}$$

The model details and assumptions are described in the followings with model variables and constants listed in Table 1.

(1) It is a one-dimensional model since the thickness of MEA (cathode or anode: about 7 μm; membrane: about 30 μm) is much thinner than MEA in-plane dimensions (5 cm × 5 cm). And in-plane uniformity is assumed.
(2) The cathode includes Pt/C solid phase uniformly mixed with Nafion® electrolyte and gas pore phase. The polymer (and/or ionomer) volume fractions were assumed to be 30% (ε_C) in the cathode and 100% (ε_M) in Nafion® membrane.
(3) Pt particles are uniformly distributed across the cathode. In principle, any Pt particle size distribution can be simulated. For this degradation mechanism focused study, we adopted a simple bi-modal particle size distribution: small particles with the particle size R_S and large particles with the size of R_L, which also allowed us to observe the particle size effects on degradation behaviors. All Pt particles are assumed to be spherical. The radius of particle represents the Pt metal core, excluding the surface Pt oxide. Pt dissolution (Eqs. (1) and (2)) and oxidation (Eqs. (3) and (4)) rates are expressed by the modified Butler–Volmer equations with electrochemical potentials adjusted based on particle radius by the Kelvin equation assuming constant surface properties (Eqs. (2) and

Table 1
Model variables and constants

Variables constants	Units	Physical meaning
A	m^2	MEA in-plane area ($25\,cm^2 = 2.5E-3\,m^2$)
A_S, A_L	$m^2\,m^{-3}$	Specific surface areas of small and large Pt particles
C	$mol\,m^{-3}$	Pt ion concentration
CH	Unitless	Relative proton activity (1 M/1 M = 1)
C_{Ref}	$mol\,m^{-3}$	Concentration reference value ($1\,M = 1000\,mol\,m^{-3}$)
D	$m^2\,s^{-1}$	Pt ions diffusion coefficient in cathode or membrane
E	V	Externally applied potential at cathode during durability test
F	$C\,equiv^{-1}$	Faraday's constant ($96{,}485\,C\,equiv^{-1}$)
k_1	$mol\,m^{-2}\,s^{-1}$	Pt dissolution reaction rate constant
k_2	$mol\,m^{-2}\,s^{-1}$	Pt oxidation reaction rate constant
M	kg	Total Pt mass in cathode
M_{Pt}	$kg\,mol^{-1}$	Pt molecular weight ($0.1951\,kg\,mol^{-1}$)
M_{PtO}	$kg\,mol^{-1}$	PtO molecular weight ($0.2110\,kg\,mol^{-1}$)
n_1	$equiv\,mol^{-1}$	Number of equivalent electrons transferred per mole of Pt dissoluted ($2\,equiv\,mol^{-1}$)
n_2	$equiv\,mol^{-1}$	Number of equivalent electrons transferred per mole of Pt oxidized ($2\,equiv\,mol^{-1}$)
N_S, N_L	Unitless	Number of small and large Pt particles in each cathode mesh
N_{OUT}	$mol\,m^{-2}\,s^{-1}$	Pt ion diffusion flux at the cathode/membrane interface
R	$J\,(mol\,K)^{-1}$	Universal gas constant ($8.314\,J\,(mol\,K)^{-1}$)
r_{1S}, r_{1L}	$mol\,m^{-2}\,s^{-1}$	Pt dissolution rate on small and large particles
r_{2S}, r_{2L}	$mol\,m^{-2}\,s^{-1}$	Pt oxidation rate on small and large particles
RH	Unitless	Relative water activity or relative humidity
R_S, R_L	m	Radius of small and large Pt particles (exclude oxide layers) at a specific location in cathode
RR_O	m	Volume-average Pt particle radius in cathode
RR_S, RR_L	m	Volume-average small and large Pt particle radius in cathode
S	m^2	Total Pt surface area in cathode
t	s	Time
T	K	Fuel cell temperature
U_1^0	V	Standard thermodynamic potential of Pt dissolution (1.188 V)
U_2^0	V	Standard thermodynamic potential of Pt oxidation (0.980 V)
U_{1S}, U_{1L}	V	Adjusted thermodynamic dissolution potential for small and large Pt particles
U_{2S}, U_{2L}	V	Adjusted thermodynamic oxidation potential for small and large Pt particles
V	m^3	Volume of each cathode mesh
x	m	Distance away from the GDL/cathode interface in the direction across the MEA
α_{1a}	Unitless	Anodic transfer coefficient of Pt dissolution reaction
α_{1c}	Unitless	Cathodic transfer coefficient of Pt dissolution reaction
α_{2a}	Unitless	Anodic transfer coefficient of Pt oxidation reaction
α_{2c}	Unitless	Cathodic transfer coefficient of Pt oxidation reaction
ε_C	Unitless	Nafion polymer or ionomer volume fraction in cathode
ε_M	Unitless	Nafion polymer or ionomer volume fraction in membrane
Γ_{max}	$mol\,m^{-2}$	Maximum oxide at Pt surface $2.18E-5$ (atom ratio of Pt:O = 1:1)
$\Delta\mu_{Pt}^0$	$J\,mol^{-1}$	Fitted chemical potential shift for PtO
θ_S, θ_L	Unitless	Total surface oxide coverage at small and large Pt particles
θ_{max}	Unitless	Maximum surface oxide coverage at the top monolayer
θ_S^V, θ_L^V	Unitless	Pt oxide vacancy at the top surface monolayer of small and large Pt particles
ρ_{Pt}	$kg\,m^{-3}$	Pt metal density ($21{,}090\,kg\,m^{-3}$)
ρ_{PtO}	$kg\,m^{-3}$	PtO density ($14{,}100\,kg\,m^{-3}$)
σ_{Pt}	$J\,m^{-2}$	Surface tension of Pt nanoparticles ($2.37\,J\,m^{-2}$) [18]
σ_{PtO}	$J\,m^{-2}$	Surface tension of PtO nanoparticles ($1.00\,J\,m^{-2}$) [18]
ω	$J\,mol^{-1}$	PtO–PtO interaction coefficient

(4)) [18].

$$r_{1i} = k_1\theta_i^V\left[\exp\left\{\frac{\alpha_{1a}n_1F(E-U_{1i})}{RT}\right\} - \frac{c}{c_{ref}}\exp\left\{\frac{-\alpha_{1c}n_1F(E-U_{1i})}{RT}\right\}\right] \quad (1)$$

$$U_{1i} = U_{1i}^0 - \frac{1}{2F}\frac{\sigma_{Pt}M_{Pt}}{\rho_{Pt}}\frac{1}{R_i} \quad (2)$$

$$r_{2i} = k_2\,\exp\left\{\frac{-\omega\theta_i}{RT}\right\}\exp\left\{\frac{\alpha_{2a}n_2F(E-U_{2i})}{RT}\right\} - k_2c_H^2\theta_i\,\exp\left\{\frac{-\alpha_{2c}n_2F(E-U_{2i})}{RT}\right\} \quad (3)$$

$$U_{2i} = U_2^0 + \frac{1}{2F}\left[\Delta\mu_{Pt}^0 + \frac{\sigma_{PtO}M_{PtO}}{\rho_{PtO}}\frac{1}{R_i} - \frac{\sigma_{Pt}M_{Pt}}{\rho_{Pt}}\frac{1}{R_i}\right] \quad (4)$$

(4) Pt ions are dissolved in the Nafion or its ionomer phase in the cathode and in the membrane separator. Both large and small

Pt particles "see" a mixed (average) Pt ion concentration at the same location in cathode.

(5) Pt ions from the cathode are transported by diffusion into the membrane. Under the simulated potential cycling conditions [20], the potential field (Φ) in electrolyte phase is relatively weak due to the small current density (I: less than 20 mA cm^{-2}), the high electrolyte concentration and the lower cell resistance (R_{FC}). The contribution of Pt ion transport by migration was estimated to be at least one order of magnitude smaller than transport by diffusion as the ratio of diffusion to migration flux estimated to be:

$$\frac{N_{\text{diff}}}{N_{\text{migr}}} = \frac{D\nabla C}{zuFC\nabla\Phi} \approx \frac{D\nabla C}{z(D/RT)FC\nabla\Phi} \approx \frac{RT}{zF(I \times R_{FC})} \approx \frac{8.314 \times 333}{2 \times 96485 \times (0.02 \times 0.06)} \approx 12,$$

assuming Pt ion mobility (u) as diffusivity (D)/RT. Hence, migration is neglected in these simulations. At the interface between the cathode and the gas diffusion layer (GDL), the concentration gradient of Pt ions is set to be zero, *i.e.*, zero flux. Loss of platinum into the effluent product water has been determined to be insignificant in our fuel cell tests, so it is neglected in the model. A mass balance on platinum ions gives

$$\varepsilon_j \frac{\partial c}{\partial t} = D\varepsilon_j^{1.5} \frac{\partial^2 c}{\partial x^2} + \sum_{i=S,L} A_i r_1, \tag{5}$$

where $A_i = (4\pi R_i^2/V)N_i$ is the specific interfacial surface area for the platinum particles. The diffusion coefficient is adjusted by electrolyte volume fraction ε_j within region j, and assuming a tortuosity ($\tau = \varepsilon^{0.5}$).

(6) Pt ions transported into the membrane can be chemically reduced by hydrogen that permeates through the membrane from the anode, forming a Pt "band". We assume the deposited platinum atoms are located at the position predicted by the rates of permeation of hydrogen and oxygen [16]. The width of the Pt band is neglected and the concentration of Pt ion at the "band" location is set to be zero.

(7) Pt atoms on a nanoparticle surface can be electrochemically oxidized allowing more than monolayer oxide coverage, and the formed PtO can be partially or completely reduced at the reduction conditions. In the case of beyond one monolayer surface oxide coverage, platinum oxide prevents the metal underneath from continuously dissolving. Although PtO has a certain small solubility, chemical dissolution of PtO is not treated due to its unknown kinetics.

(8) The number of each type of Pt particles is held constant (50% each type), but the sizes of these particles are allowed to change during degradation. When small Pt particles shrink and become platinum clusters, for example, a 7-atom Pt cluster with an estimated radius of 0.3 nm, no special treatment is introduced due to the limited understanding so far. The volume-average overall (RR_O), small (RR_S), and large (RR_L) Pt particle radii in cathode are calculated by Eqs. (6) and (7). The definition of volume-average overall particle radius (RR_O), different from the defined average particle size consistent to uniform particle size distribution in Darling and Meyers's model [19], allows direct comparison to average particle size measured by X-ray diffraction.

$$RR_O = \frac{\sum_x \sum_{i=S,L} N_{x,i} R_{x,i}^4}{\sum_x \sum_{i=S,L} N_{x,i} R_{x,i}^3} \quad (x : \text{location in cathode}). \tag{6}$$

$$RR_i = \frac{\sum_x \left(N_{xi} R_{x,i}^4\right)}{\sum_x \left(N_{x,i} R_{x,i}^3\right)} (i = S, L) \tag{7}$$

The total platinum particle surface area is given by

$$S = \sum_x \sum_{i=S,L} 4\pi N_{x,i} R_{x,i}^2, \tag{8}$$

but this area neglects the surface oxide layer. The loss of measured electrochemical surface area (in the unit of m^2 instead of typical m^2 g^{-1} Pt, due to unknown Pt mass in cathode with degradation) can be compared with the simulated results. The total mass of Pt is simply the initial mass minus that which diffuses away over the course of the simulation;

$$M(t) = M(t=0) + A \int_0^t \varepsilon_M D \left.\frac{\partial c}{\partial x}\right|_{x=L} \mathrm{d}t. \tag{9}$$

The set of partial differential equations with boundary conditions are linearlized, cast in finite difference form, and solved numerically. The Crank–Nicolson implicit method was used to evaluate the derivatives with time. Due to the different electrolyte volume faction in the cathode and the membrane, Pt ion mass balance in the interface is dealt with the control volume method.

3. Results and discussions

Fig. 1 shows the simulated and measured fuel cell cathode cyclic voltammetry (CV) curves at 60 °C and fully humidified conditions with a sweep rate of 50 mV s^{-1} from 0.4 to 1.0 V (vs. reference hydrogen electrode: RHE). The charging and decharging currents in the experimental curve were removed for an easy comparison. Hydrogen adsorption and de-sorption, which occur at potentials below 0.4 V (vs. RHE), were not simulated. Pt dissolution currents for all assumed or fitted kinetics cases in this work were at least two orders of magnitude lower than Pt oxidation currents, hence not affecting the CV curve shapes. The simulated CV curve fits the measured one well with the slightly different curve shapes when the oxidation plateau current is reached. Similar CV simulation results were presented by Darling and Meyers [18]. However, our fitted oxidation reaction rate constant (k_2) was higher than the other reference values as shown in Table 2, mostly due to the different nature of Pt electrode (either Pt wire or Pt/C nanoparticles), the different Pt nanoparticle sizes and the simulated experimental conditions

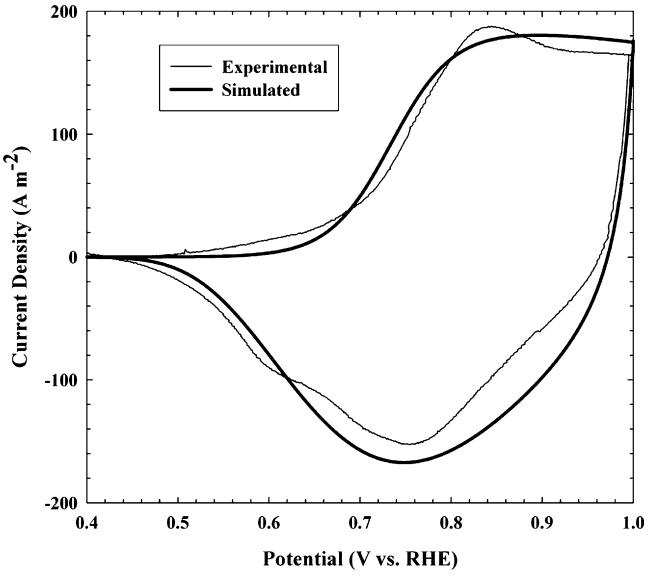

Fig. 1. Simulated and experimental Pt/C electrode cyclic voltammetry curves.

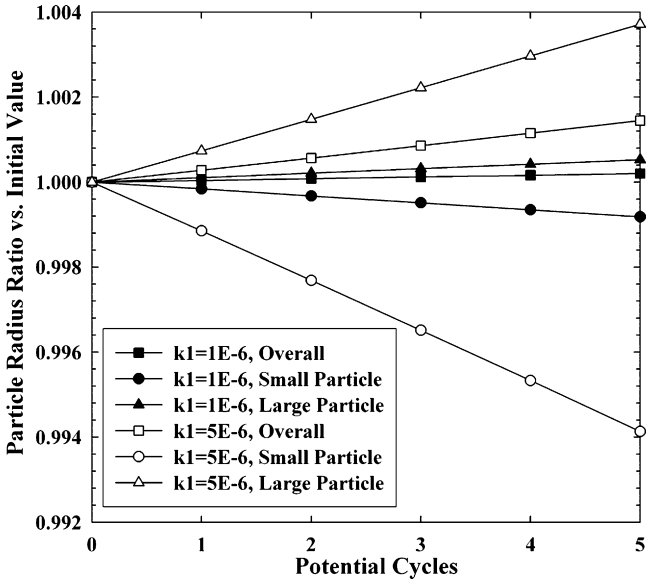

Fig. 2. Simulated overall, small and large Pt particle size changes in cathode during potential cycling under no Pt ion diffusion conditions.

(cell temperatures). Other fitted Pt oxidation parameters were very close to the literature values.

These fitted Pt oxidation parameters were then adopted for use in the cathode catalyst degradation model. Accelerated catalyst degradation testing was simulated and compared with experiment. The cathode potential was cycled between 0.87 and 1.20 V (vs. RHE) with a step time 30 s (1 min per cycle) at 60 °C and fully humidified conditions. The cathode electrochemically active surface area (ECA) was measured periodically during degradation. After the completion of potential cycling, the Pt particle size in the cathode was measured by X-ray diffraction, and the mass distributions determined through SEM-EDS analysis of MEA cross-sections [16]. The experimental details and results were presented previously [20]. In this simulation, we used a simplified bi-modal particle size distribution with equal numbers of the small and large Pt particles. The assumed representative initial particle radii were 1.50 and 1.75 nm for the small and large particles respectively, which matches the volume-average value of 1.65 nm in a fresh cathode measured by X-ray diffraction. The sensitivity of catalyst degradation rates on the initial Pt particles radii and the number percentage for each type particle was not investigated.

Previous modeling results [19] showed decreasing particle radii, which might be caused by an overemphasis on Pt cation transport in MEA. Therefore, we first simulated catalyst degradation without the Pt ion diffusion and subsequent hydrogen reduction processes. Under these conditions, both the small and large Pt particle radii remained uniform across the cathode during the simulation. The volume average overall Pt particle radius (RR_O) increased with potential cycling as shown in Fig. 2. Since the driving force for electrochemical dissolution of Pt increases with decreasing Pt particle size [21], the smaller Pt particle has a higher Pt dissolution rate during the anodic sweep, and a lower Pt ion deposition rate during the cathodic sweep. Hence, small Pt particles shrank during potential cycling due to a net Pt mass loss through Pt dissolution, and large particles grew with a net gain by Pt ion deposition. An increase of the

Table 2
Fitting parameters

Parameter	Fitted value	Adopted value	Other values in literature
U_1^0		1.188 V [1]	
α_{1a}	0.5		
α_{1c}	0.5		
U_2^0		0.98 V [1]	
α_{2a}	0.4		0.25–0.45 [8]; 0.35 [18]
α_{2c}	0.1		0.15 [18]
$\Delta\mu_{Pt}^0$	$-38\,kJ\,mol^{-1}$		$-42.3\,kJ\,mol^{-1}$ [18]
σ_{Pt}		$2.37\,J\,m^{-2}$ [18]	
σ_{PtO}		$1.00\,J\,m^{-2}$ [18]	
ω	$30\,kJ\,mol^{-1}$		$24–35\,kJ\,mol^{-1}$ [8]; $30\,kJ\,mol^{-1}$ [18]
k_1	$3\times10^{-6}\,mol\,m^{-2}\,s^{-1}$		$3.4\times10^{-9}\,mol\,m^{-2}\,s^{-1}$ [18]
k_2	$7\times10^{-6}\,mol\,m^{-2}\,s^{-1}$		1.0×10^{-9}–$1.0\times10^{-14}\,mol\,m^{-2}\,s^{-1}$ [8]; $1.36\times10^{-7}\,mol\,m^{-2}\,s^{-1}$ [18]
R (initial)	1.65 nm (XRD observed)		

dissolution rate constant (k_1) resulted in the faster Pt dissolution and Pt ion deposition rates; thus, faster Pt mass exchange between small and large particles, and a faster overall Pt particle size growth rate. These simulations confirm that in the absence of platinum diffusion the expected changes in particle size occur.

In fact, significant loss of cathode Pt mass was observed [20] experimentally under potential cycling. Since negligible platinum is found in the water, the loss of platinum from the catalyst layer is presumably due to Pt ion transport and its deposition by hydrogen reduction in membrane. Unfortunately, the diffusivity of the Pt ion in Nafion® membrane or equivalent ionomer has not been reported. During the potential cycling, fluoride ion concentrations in waste water from both the anode and cathode were measured by ICS-2000 Ion Chromatography System (Dionex Corporation). The levels typically measured, 10–200 ng g^{-1} (ppb), were much higher than the detected Pt concentrations (<10 ppt). Although there could be some concentration differences between the liquid phase (waste water) and the solid phase (Nafion® electrolyte) for both fluoride ions and soluble Pt species, it is very likely that $(PtF_x)^{n-}$ complexes can be formed even with a relatively weak chelating ability of fluoride ion. The negatively charged $(PtF_x)^{n-}$ complexes could slow down the Pt ion diffusion. The effective diffusivity of Pt^{4+} ion complex $(PtCl_6)^{2-}$ in Nafion® 117 membrane was measured about 1.4×10^{-12} m^2 s^{-1} [22], which is much smaller than the assumed value of 10^{-10} m^2 s^{-1} (already one order of magnitude smaller than that of Pt ions in water) in Darling and Meyers's simulation work [19].

With a Pt ion diffusivity of 10^{-10} m^2 s^{-1} and an assumed Pt dissolution rate constant ($k_1 = 5 \times 10^{-9}$ mol m^{-2} s^{-1}) close to Darling and Meyers's fitted value, the simulated cathode Pt surface area had a negligible loss under the potential cycling conditions. The measured ECAs for the fresh and the degraded (after 300 and 1000 potential cycles) cathodes are plotted in Fig. 3 with a linear interpolation between experimental data points. These data, in fact, show significant loss surface area with potential cycling. Similarly these assumed Pt ion diffusivity and Pt dissolution rate constant yielded no significant Pt mass loss in the cathode as shown in Fig. 4. The estimated Pt mass in the cathode was presented in our previous work based on the SEM-EDS measurements before and after potential cycling [20]. Compared to Darling and Meyers's simulation results [19], these much lower surface area and mass loss rates were caused by the smaller Pt ion concentration due to the faster Pt oxidation rate with higher oxide coverage. With potential cycling, the simulated overall Pt particle radius actually decreased slightly as shown in Fig. 5, similar to Darling and Meyers's simulation results [19]. Such particle shrinking behaviors were due to the relatively faster Pt ion transport than Pt dissolution and deposi-

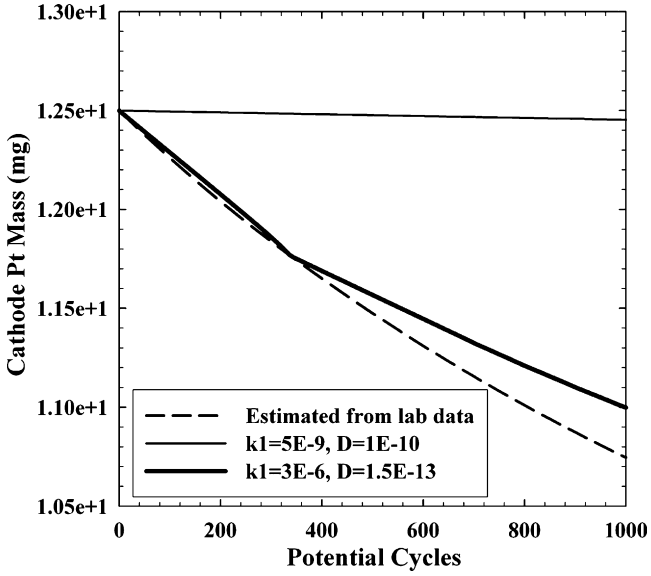

Fig. 4. Simulated cathode Pt mass loss during potential cycling with calculated values based on lab data [20].

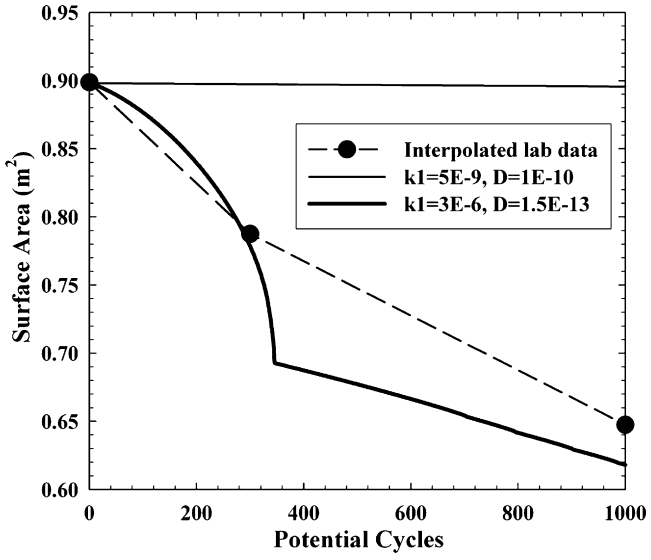

Fig. 3. Simulated cathode Pt surface areas under potential cycling with linearly interpolated measured electrochemically active surface area.

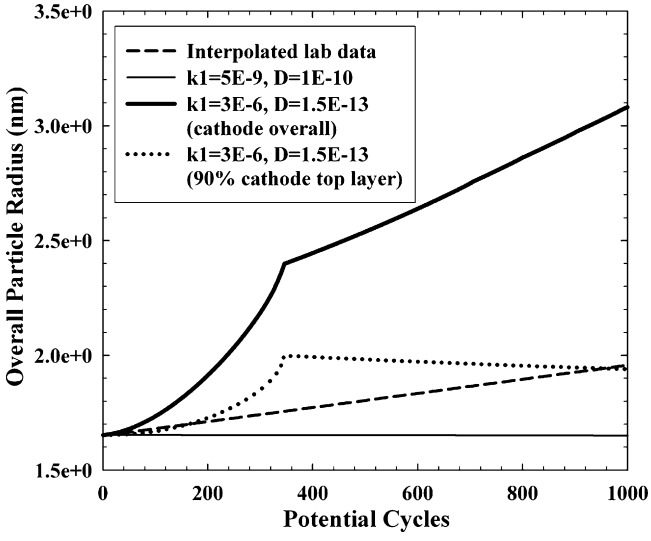

Fig. 5. Simulated overall cathode Pt particle radius during potential cycling with linearly interpolated data of fresh and degraded cathode measured by X-ray diffraction.

tion processes, which could even result in both small and large Pt particle size decrease.

Since the cathode Pt mass loss rate depends on both Pt ion diffusivity and ion concentration, the Pt dissolution rate constant was increased and Pt ion diffusivity was decreased to match Pt mass loss and particle growth behaviors. With the adjusted Pt ion diffusivity ($1.5 \times 10^{-13}\,m^2\,s^{-1}$) and Pt dissolution rate constant ($3 \times 10^{-6}\,mol\,m^{-2}\,s^{-1}$), the cathode surface area loss rate had a similar magnitude as the measured data as shown in Fig. 3. However, the simulated surface area profile had an initial concave-down shape with the dramatic surface loss after 300 potential cycles. This was caused by the accelerated dissolution rate for the small Pt particle with decreasing size. Fig. 6(a) shows the small Pt particles at the cathode center shrank at an increasing rate until reaching a size of 0.15 nm, at about 350 potential cycles. During the further potential cycling, the small Pt clusters (except those close to the cathode/membrane interface) will be fully covered with oxide even after 30 s of reduction phase at 0.87 V, which is still much higher than the adjusted dissolution thermodynamic potential (lower than 0.5 V for such a small cluster). So these small Pt clusters only experienced oxidation and oxide reduction without mass losses by dissolution, thus the size remained as constant. Presumably, these small particles can diffuse, but coarsening of these Pt clusters was not treated in this work.

The Pt mass loss in the cathode matched the estimated values from measured data as shown in Fig. 4. However, the overall Pt particle growth rate was much faster than the estimated rate by linearly interpolating the measured particle determined from X-ray diffraction before and after degradation by (Fig. 5). Since a small X-ray incident angle (1°) was applied on the cathode layer in MEA to avoid collecting the diffracted signals from Pt particles in Pt "band" (only about 5.5 μm away from the cathode/membrane interface), Pt particles in the cathode close to the cathode/membrane interface might not be well detected by X-ray. To account for this possible effect, Pt particles in the 90% of the cathode top layer were used to calculate the volume-average particle size, which showed a better matching. The volume average particle size quickly approached the large particle size as shown in Fig. 6(b). This is attributed to the fact that small Pt particles are less weighted in the calculation of volume-average particle size. The larger particles produced at the cathode/membrane interface as shown in Fig. 6(a and b) were caused by the Pt ion diffusion back from the membrane and deposition at the interface region during the reduction period of the potential cycling. The Pt ion concentration spatial profiles during the 100th potential cycle are plotted in Fig. 7. The cathode thickness was 7 μm and the Pt band located in the membrane 5.5 μm away from the cathode–membrane interface. Due to the high dissolution rate and low Pt ion diffusivity, Pt ion concentration in membrane is much higher than that in the cathode

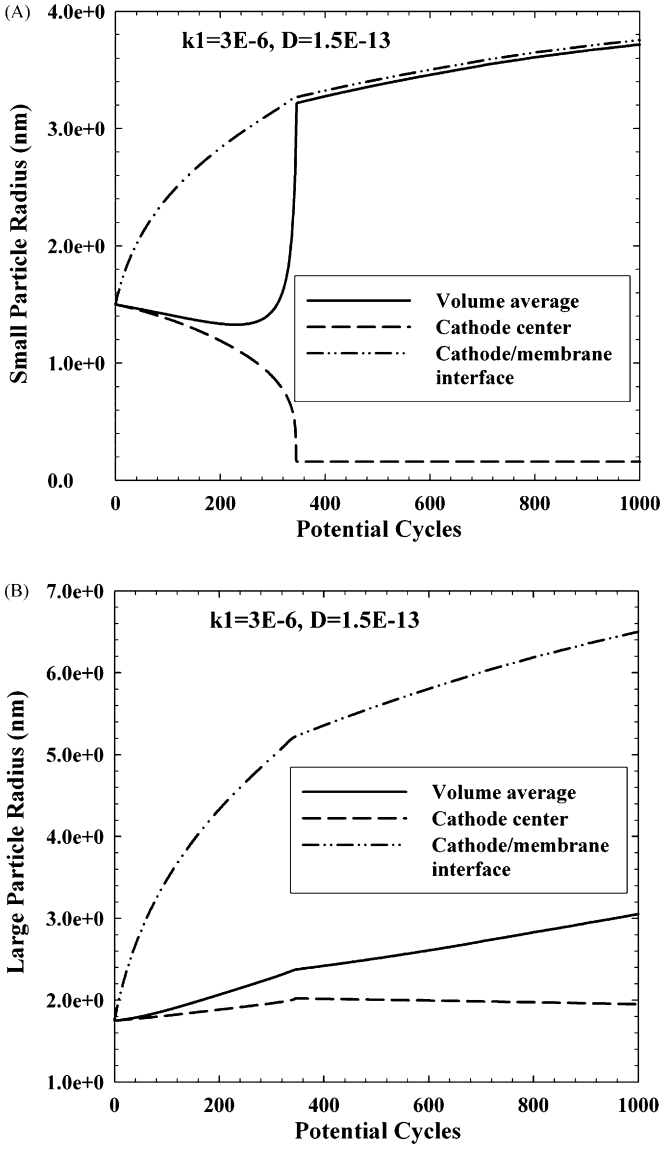

Fig. 6. (a) Simulated volume average radius of small Pt particle in cathode and Pt radius at cathode center and cathode–membrane interface. (b) Simulated volume average radius of large Pt particle in cathode and Pt radius at cathode center and cathode–membrane interface.

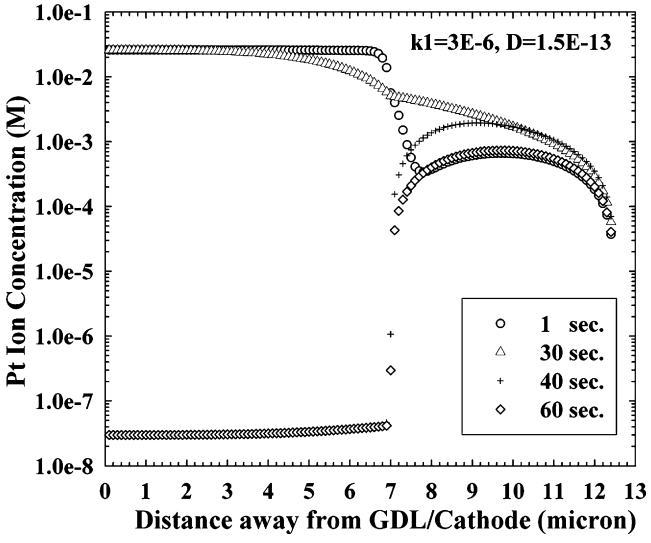

Fig. 7. Simulated Pt ion concentration spatial profiles during the 100th potential cycle (cathode thickness: 7 μm).

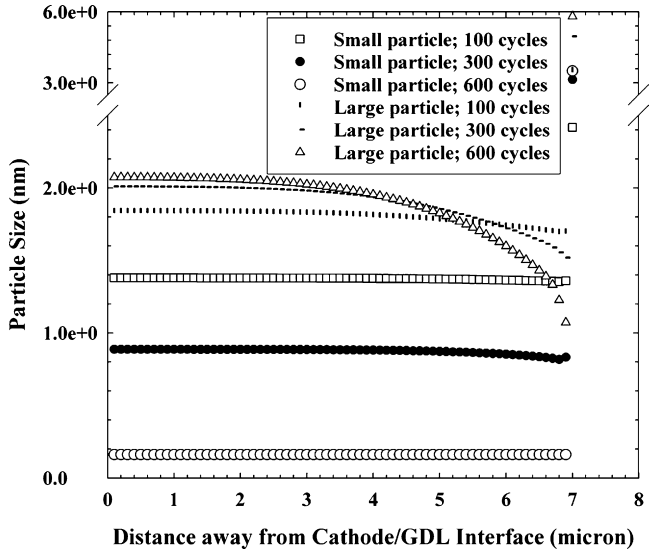

Fig. 8. Simulated cathode Pt particle size spatial profiles during potential cycling (cathode thickness 7 μm).

during the reduction period (the second 30 s of the 1-min potential cycle) resulting in Pt ion in the membrane diffusing towards both the cathode and the Pt band location to be reduced electrochemically or chemically by hydrogen, respectively. Fig. 8 shows the Pt particle spatial profiles with the decreased sizes of large Pt particles towards the cathode/membrane interface. This was caused by the rapid particle growth at the interface which drove the surrounding particles shrinkage. Since small particle shrank with degradation, its size distribution across the cathode was more uniform with only a small dip close to interface region.

Pt particle growth at cathode/membrane was not investigated in our experiments; however, the simulated particle size spatial profiles contradict Ferreira's observations [2]. So it seemed that the Pt ion concentration shown in Fig. 7 was unlikely high during the anodic period of the potential cycling. The assumed effective Pt ion diffusivity with porosity and tortuosity correction is two orders of magnitude lower than the measured diffusivity of $(PtCl_6)^{2-}$ complex in Nafion® electrolyte [22]. Even with the further parameter adjustment, this proposed Pt/C catalyst degradation model will lead to the small Pt particle quickly decreasing in size decrease. This results in a dramatic surface area loss and a sharp increase in the overall particle size after the small particles reach the sub-nanoparticle region. This is also partly due to the untreated neighboring Pt clusters or sub-nanoparticles coarsening in the model. So our simulation results suggest that degradation processes besides Pt dissolution and Pt ion deposition are important in catalyst degradation. Also, the model assumption that Pt ion electrochemical deposition solely on Pt metals excludes the nucleation of fresh Pt particles or clusters on carbon support. In fact, More's experimental work also suggests that new Pt nanoparticle formation during catalyst degradation [17]. With the added features of new Pt cluster formation and its coarsening in a future model, small Pt particles will not diminish with catalyst degradation. It is likely that with reasonable Pt ion concentration and Pt ion diffusion rate that Pt particle growth and losses of catalyst surface area and cathode Pt mass could be well predicted.

4. Conclusions

A physics-based model of catalyst degradation was proposed for platinum supported on carbon for a PEM fuel cell. The following processes have been treated in the model: (1) electrochemical dissolution and re-deposition in the cathode; (2) Pt ion transport by diffusion in MEA; and (3) Pt ion chemical reduction in membrane by hydrogen that permeates from the anode. A simplified bi-modal particle size distribution was adopted to simulate the overall cathode Pt particle growth, surface area loss and Pt mass loss. Overall Pt particle growth by Pt mass exchange between small and large particles was clearly demonstrated through Pt dissolution and Pt ion deposition. In this initial study, a simplified model was developed to elucidate cathode catalyst degradation. Further refinements are needed to describe more accurately cathode degradation behavior in order to predict degradation over typical lifetimes of PEMFCs. The degradation model did not well predict Pt catalyst degradation rate with the reasonable parameters. It seemed that the assumed Pt ion diffusion rate was too low and Pt ion concentration was too high. We concluded that additional mechanism besides Pt dissolution and Pt ion deposition involve in the catalyst degradation process. Catalyst degradation processes of Pt cluster formation on carbon support and neighboring Pt clusters and/or nanoparticles coarsening were proposed for further experimental and simulative investigation.

Acknowledgement

This work was supported by the Toyota Motor Engineering & Manufacturing North America, Inc.

References

[1] M. Pourbaix, Atlas of Electrochemical Equilibria in Aqueous Solution, Pergamon Press, Oxford, 1966.
[2] P.J. Ferreira, G.J. La, O.Y. Shao-Horn, D. Morgan, R. Makharia, S. Kocha, H.A. Gasteiger, J. Electrochem. Soc. 152 (2005) A2256.
[3] X. Wang, R. Kumar, D.J. Myers, Electrochem. Solid-State Lett. 9 (2006) A225.
[4] D.C. Johnson, D.T. Napp, S. Brunckenstein, Electrochim. Acta 15 (1970) 1493.
[5] D.A.J. Rand, R. Woods, J. Electroanal. Chem. 35 (1972) 209.
[6] K. Kinoshita, J.T. Lunqdist, P. Stonehart, J. Electroanal. Chem. Interfacial Electrochem. 48 (1973) 157.
[7] B.E. Conway, B. Barnett, H. Angerstein-Kozlowska, B.V. Tilak, J. Chem. Phys. 93 (1990) 8361.
[8] D.V. Heyd, D.A. Harrington, J. Electroanal. Chem. 335 (1992) 19.
[9] C.H. Paik, T.D. Jarvi, W.E. O'Grady, Electrochem. Solid-State Lett. 7 (2004) A82.
[10] M. Alsabet, M. Grden, G. Jerkiewicz, J. Electroanal. Chem. 589 (2006) 120.
[11] H. Xu, R. Kunz, J.M. Fenton, Electrochem. Solid-State Lett. 10 (2007) B1.
[12] G. Jerkiewicz, G. Vatankhah, J. Lessard, M.P. Soriaga, Y.-S. Park, Electrochim. Acta 49 (2004) 1451.
[13] P.J. Ferreira, Y. Shao-Horn, Electrochem. Solid-State Lett. 10 (2007) B60.
[14] K. Yasuda, A. Taniguchi, T. Akita, T. Ioroi, Z. Siroma, Phys. Chem. Chem. Phys. 8 (2006) 746.

[15] A. Ohma, S. Suga, S. Yamamoto, K. Shinohara, ECS Trans. 3 (2006) 519.
[16] W. Bi, G.E. Gray, T.F. Fuller, Electrochem. Solid-State Lett. 10 (2007) B101.
[17] K.L. More, K.S. Reeves, DOE Hydrogen Program Review, 2005.
[18] R.M. Darling, J.P. Meyers, J. Electrochem. Soc. 150 (2003) A1523.
[19] R.M. Darling, J.P. Meyers, J. Electrochem. Soc. 152 (2005) A242.
[20] W. Bi, T.F. Fuller, ECS Trans. 11 (2007) 1235.
[21] C.T. Campbell, S.C. Parker, D.E. Starr, Science 298 (2002) 811.
[22] M.S. Kang, Y.I. Joe, J. Power Sources 77 (1999) 49.